Geotextiles and Geomembranes 46 (2018) 190–205

Contents lists available at ScienceDirect

Geotextiles and Geomembranes

journal homepage: www.elsevier.com/locate/geotexmem

Use of cellular confinement for improved railway performance on soft subgrades

Sagar Raj Satyal[a], Ben Leshchinsky[b,*], Jie Han[c], Madan Neupane[d,e]

[a] Oregon State University, 101 Kearney Hall, Corvallis, OR 97331, United States
[b] Oregon State University, Department of Forest Engineering, Resources and Management, 204 Peavy Hall, Corvallis, OR 97331, United States
[c] Glenn L. Parker Professor of Geotechnical Engineering, The University of Kansas, 1530 W. 15th St., Lawrence, KS 66045-7609, United States
[d] Gannett Fleming, Inc., 5 Eves Drive Suite 200, Marlton, NJ 08053, United States
[e] The University of Kansas, 1530 W. 15th St., Lawrence, KS 66045-7609, United States

ABSTRACT

Due to extensive right-of-way, railroads are inevitably subject to poor subgrade conditions and interrupted service for significant maintenance due to excessive deformations and loss of track geometry. Geocell confinement presents itself as a possible solution for improving performance of ballasted railroad embankments over weak subgrade. To investigate the efficacy of geocell confinement on ballasted railway embankments, a set of well-instrumented, large-scale cyclic plate loading tests and numerical simulations were performed on geocell-confined ballast overlaying a weak subgrade material. The agreement of results from tests and simulations served as a basis for simulating practical track geometry and performance for various geocell configurations and subgrades using three-dimensional (3D) finite element (FE) analyses. The study showed that geocell reinforcement significantly decreased track settlement, decreased subgrade deformations with lower and uniform distribution of vertical stresses on subgrade and inhibited lateral deformation and serviceability under cyclic loading. These results demonstrate that geocell confinement can be an effective alternative to subsurface improvement or shorter maintenance cycles, particularly on weak subgrades.

1. Background

Cellular confinement, or geocell, is a three-dimensional (3D) honeycombed shaped geosynthetic used to increase the strength and modulus of the cohesionless soils through a mechanism of confinement. In cohesionless soils, such as sands or gravels, shear strength and modulus are generally low under small confining pressures, but can be increased using additional confinement offered by a geocell structure under small deformations. Geocell is more effective for soil confinement than other types of geosynthetics (e.g., geogrid or geotextile through interlocking or friction), making it the subject of extensive study as the complex interdependence of geometry, soil strength and loading mechanism make its composite behavior difficult to quantify.

The US Army Corps of Engineers first investigated cellular confinement as a construction concept to economically improve mobility for roads across soft ground (Webster and Alford, 1978) and concluded cellular confinement, initially done with aluminum, increased soil strength under loading. The soil was compacted in the cellular grids and test traffic was applied over the soil to test the effectiveness of geocell confinement. The enhanced confining effects of geocell on aggregate materials were later observed through use of large-diameter triaxial tests, demonstrating notable increases in strength (Bathurst and Karpurapu, 1993). Similar triaxial tests have demonstrated increased strength of granular soils with geocell confinement (Biabani et al., 2016a), some electing to analyze its effects as an apparent cohesion for simplicity (Rajagopal et al., 1999). However, the geocell increases the strength of granular materials through enhanced confinement effects, which also stiffens the reinforced composite through a “mattress” effect (Zhou and Wen, 2008; Hegde, 2017), especially beneficial over soft soil (Biswas and Krishna, 2017). Geocell reinforcement has demonstrated increased strength and reduced deformation over a variety of adverse soil conditions; however its implementation is limited due to lack of comprehensive design methods (Yuu et al., 2008; Hegde, 2017).

Geocells are usually shipped in folded form and are spread during installation to form a honeycomb like structure with pockets (cells) into which soil is added and compacted. The three-dimensional shape of the cells (each pocket) provides the confinement effects to the soil by surrounding it thus creating a stiff structure that prevents lateral movement of material, consequently increasing soil strength (Koerner, 2012). This system has demonstrated effectiveness in increasing the

* Corresponding author.
E-mail addresses: satyals@oregonstate.edu (S.R. Satyal), ben.leshchinsky@oregonstate.edu (B. Leshchinsky), jiehan@ku.edu (J. Han), mneupane@gfnet.com (M. Neupane).

https://doi.org/10.1016/j.geotexmem.2017.11.006
Received 29 August 2016; Received in revised form 26 November 2017; Accepted 27 November 2017

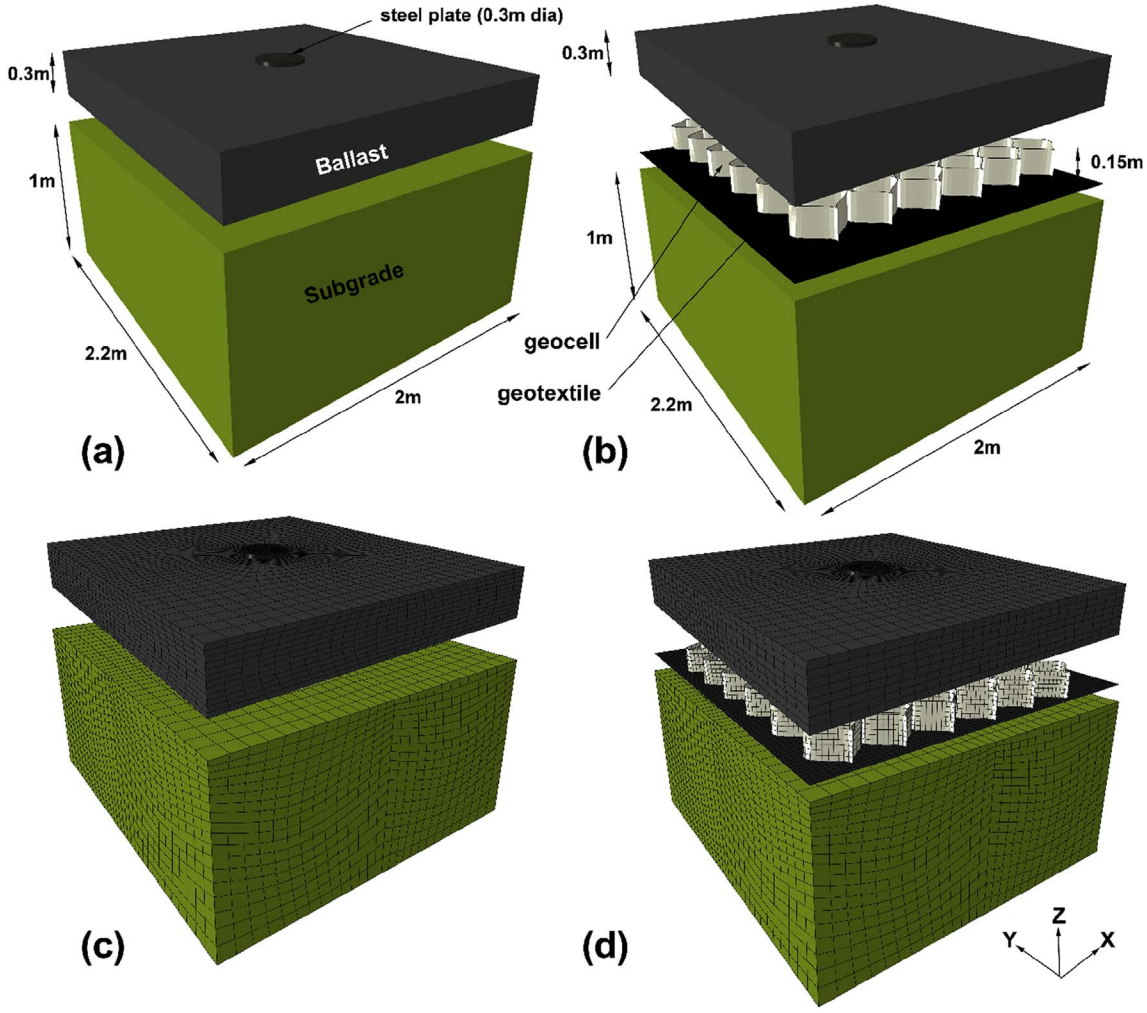

Fig. 1. Details of plate loading tests and respective (a) Unreinforced, (b) Reinforced models geometry and mesh for respective (c) Unreinforced and (d) Reinforced models.

strength of soil, particularly cohesionless soil, reducing deformations under monotonic and cyclic loading (Leshchinsky, 2011; Biabani et al., 2016b; Thakur et al., 2016; Pokharel et al., 2017). Large scale triaxial tests conducted on geocell-reinforced sub-ballast subjected to cyclic loading showed that the increased confinement reduced the vertical and volumetric strains in the sub-ballast. Benefits of using geocell was noticeably higher at the low confining pressures at higher frequency of loading (Indraratna et al., 2015).

Numerical modelling of geocell has been a notable challenge due to its complex, three-dimensional honeycomb structure. Hegde and Sitharam (2015) modelled the 3D honeycomb shape of the geocells using Finite Element (FE) analysis and found that reinforcements were effective in distributing loading to a wider area and to a relatively shallow depth as compared to unreinforced soil and geogrid-reinforced soil. Han et al. (2008) carried out mechanistic analysis of a geocell-reinforced gravel base over soft subgrade under a vertical loading using the finite difference method, demonstrating that geocell confinement improved load-bearing behavior. Leshchinsky and Ling (2013a; 2013b) performed laboratory and numerical analyses of railway ballast embankments reinforced with geocell under monotonic and cyclic loading conditions, demonstrating improved load-carrying capacity and inhibited lateral displacements for ballast embankments. Numerical models and experiments both showed geocell confinement minimized settlement under both cyclic and monotonic loads. However, damage was noted at the seams of the geocells used in these tests (Leshchinsky and Ling 2013a,b) under higher loading – a by-product of the manufacturing process. In the tests outlined within this study, no significant damage (tearing, rupture) was noted at the seams.

Ballast performs many important functions for railroad performance, including resisting vertical, lateral and longitudinal forces, absorbing energy and reducing vibrations, providing adequate drainage, and distributing the load from the railroad to acceptable levels for the subgrade (Selig and Waters, 1994). Due to the repeated loads incurred over many cycles, rearrangement and degradation of ballast occurs. This results in ballast fouling and loss of geometry due to lateral spreading of the ballast (Lackenby et al., 2007). The degradation of ballast causes reduced frictional strength and increased lateral spreading which is regarded as the primary cause of loss of track geometry and causes higher track maintenance cost. Geocell reinforcement has been used in various geotechnical applications and has shown improvement in performance but studies of geocell reinforcement in railway embankments are limited (Indraratna et al., 2015). Geocells have shown to improve the settlement behavior of soil due to increased strength and stiffness of the reinforced mattress (Zhou and Wen, 2008), resulting in lower displacements and wider distribution of loading (Yang et al., 2010) causing lower shear stresses at the subgrade interface (Giroud and Han, 2004). In full-scale railway testing, geocell resulted in sustained track geometry stemming from reduced settlement and lateral spreading (Raymond, 2001). Insight into the performance improvements stemming from geocell reinforcement of ballasted railway embankment overlying weak subgrades is limited. However, numerical simulations based on physical experiments are a useful means for investigating design considerations pertaining to geocell-reinforced railway embankments in a controlled manner without the

expense and labor required for full-scale field tests. Furthermore, the findings are illustrative for designing for better railway performance and reduced track maintenance cost.

In this study, two plate loading tests were carried out on a large-scale soil box infilled with a soft subgrade and a ballast layer with or without geocell confinement. During these tests, displacements, stresses and actuator load were monitored for 6000 cycles of loading. The results of these tests and their corresponding material properties were used as a baseline for developing 3D finite element models to assess the simulated behavior of ballast railway prisms reinforced with and without geocell over soft soil. This study expands on the work of Leshchinsky and Ling (2013a, 2013b) in that it is based on physical experiments with actual subgrade soil with an intensive pressure and displacement monitoring program. Furthermore, the numerical modelling advances upon the previous work as it accounts for plastic deformation in subgrade soils based on CBR; Leshchinsky and Ling (2013a) used an elastic subgrade, only varying stiffness. This study also accounts for a greater range in track geometries and geocell placement while also more robustly capturing the realistic geocell shape and subsurface response.

2. Laboratory experiments and numerical models

2.1. Experimental setup

A Kaolin-Sand mixture and AREMA 4A standard track ballast were placed in a reinforced steel box that was 2 m wide x 2.2 m long x 2 m deep. The box walls were made out of 25 mm thick steel sections reinforced with transverse steel I beams for rigidity. The details of the plate loading test geometry and respective FE model along with meshing are shown in Fig. 1. A loading plate attached to an MTS 245 kN hydraulic actuator was used to provide cyclic loading at 1 Hz frequency with 1000 cycles for each loading step. The waveform of the load applied was that of a haversine function, shown in Fig. 2a, and complete loading sequence for the test is shown in Fig. 2b. For the finite element analyses, a general purpose finite element software, ABAQUS (Hibbitt et al. 2007) was used. Three-dimensional FE analyses were carried out to simulate the tests and the validated model was used in an extensive parametric study to investigate the reinforcement benefits of geocell.

2.2. Materials

The ballast used for testing was trap rock aggregate (Rhyolite) from Middle Brook, Missouri and uniformly graded, meeting AREMA 4A standard track ballast specifications. The ballast had a mean grain size of D_{50} = 32 mm and maximum and minimum densities of 1525 kg/m^3 and 1340 kg/m^3 respectively as determined using ASTM D4253 Guidelines. The particle size distribution of the ballast is shown in Fig. 3. The subgrade material was prepared by mixing 20% Kaolin with 80% Kansas River Sand. The mean grain size of Kansas River Sand was 2.6 mm with sub-rounded particle shape. The plastic and liquid limits of the subgrade were 18 and 26 (ASTM D4318-10). For this material, the unconfined compressive strength (ASTM D2166/D2166M-16) versus California Bearing Ratio (CBR) (ASTM D1883) is shown in Fig. 4. The density of the subgrade was 2162 kg/m^3 (ASTM D1556/D1556M) corresponding to a CBR of 3%. The corresponding unconfined compressive strength of the subgrade was approximately 75 kPa for CBR of 3%. To achieve specifications, compaction of both the ballast and subgrade was carried out using a vibratory handheld plate compactor. The placement density was controlled using the volume-mass method. The ballast was compacted with four to five passages of the compactor to reach approximately the maximum density of each lift (150 mm). This lift thickness was selected based on the plate compactor's capacity that was deployed on the tests. No density measurements at specific locations were measured due to the difficulties in accurate measurement; therefore, no coefficient of variation of the ballast density was calculated. During compaction of angular ballast, breakage of asperities can result in more rounded grains and lower strength. Within this series of tests, there was little ballast breakage observed during compaction. For the reinforced test, a polyethylene woven geotextile was placed on the ballast-subgrade interface for separation purposes. After the placement of the geotextile, geocell was placed and filled with ballast, which was subsequently compacted in individual geocell with a hand-held pneumatic tamper to its maximum density same as that in the unreinforced test. The geocells were manufactured using polyethylene polymer with density of 935 kg/m^3 – 964 kg/m^3 (Presto GeoSystems GeoWeb) with a nominal dimension of 287 mm in width by 320 mm in length and a pocket depth of 150 mm. The details of material properties are shown in Table 1.

2.3. Material models

Three-dimensional numerical models of both the experimental setup and railway geometry were created using commercially-available finite element software (ABAQUS Explicit, Hibbitt et al. 2007). The ballast was modeled as a non-associative elastic-plastic material using hyperbolic 3D Drucker-Prager (D-P) yield criterion. Since no explicit testing of ballast strength was performed, the ballast shear strength properties were obtained from the literature (Ahlf, 1975; Indraratna and Nimbalkar, 2013; Leshchinsky and Ling, 2013b). The elastic modulus for ballast was obtained from Indraratna et al. (1998, 2015) and the elastic modulus of subgrade was obtained from Skempton (1951) using the unconfined compressive strength of the subgrade. Although the stiffness of the material properties can influence observed results, this influence was found to be relatively small in comparison to much of the plastic deformation observed in modeling.

The soft subgrade was modeled as cohesive material with negligible frictional strength (i.e. undrained conditions) using the Drucker-Prager model, an approach used by Han et al. (2008). The friction and dilation angles were set to 1° for numerical stability. Compressive strength of the subgrade material was used to model the undrained condition. The geocell and geotextiles were modeled as elastic materials which reduced computational expense and numerical difficulties. This assumption is commonly employed in similar studies as it has often been observed that strains in the geocell tend to remain within the elastic range for the given applications (Han et al., 2011; Leshchinsky and Ling, 2013a). The properties of geocell and geotextiles were obtained from Yang (2010). The elastic modulus of geocell and geotextile were estimated from tensile stiffness at 2% strain.

2.4. FE meshing and boundary conditions

In order to reduce computational expense, symmetric boundary conditions were applied and only a quarter of the box was modeled. The ballast, subgrade and loading plate were meshed using C3D8R elements (3D Plane Stress Reduced-Integration Brick Elements). The geocell and geotextile were modeled using shell elements under membrane conditions (i.e. no compressive or bending resistance), meshed with M3D4R elements (3D 4-node Reduced Integration Membrane Elements). The plate loading test model without geocell was modelled using 12924 elements and the plate loading test model with geocell was modelled using 14976 elements. Elements for the ballast had an average size of 20 mm in order to represent the size of ballast. Biased meshing was used for the subgrade to concentrate finer elements near the ballast-subgrade interface. Mesh sensitivity analyses were carried out for the model and the meshes used exhibited acceptable accuracy in comparison to meshes comprised of more elements. The vertical boundaries of the z-x plane were constrained from lateral displacement in y-direction. Similarly, the vertical planes in the outer edges of z-y planes were constrained from lateral displacement in x-direction. The base of the model was constrained from all displacements.

The interface between ballast and plate were modelled using “hard”

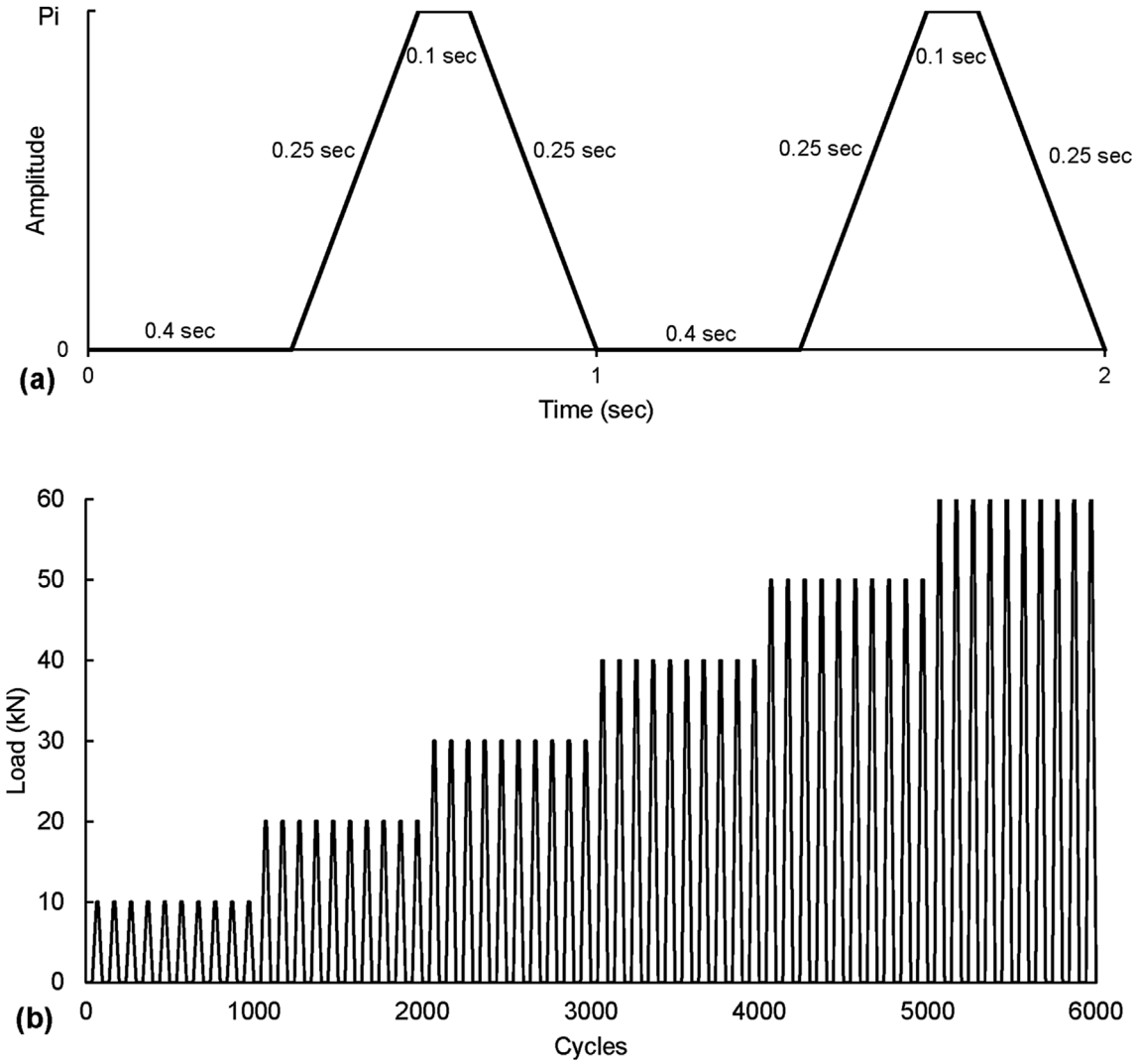

Fig. 2. (a) Haversine loading pattern used in experiments, (b) Load sequence for plate loading tests.

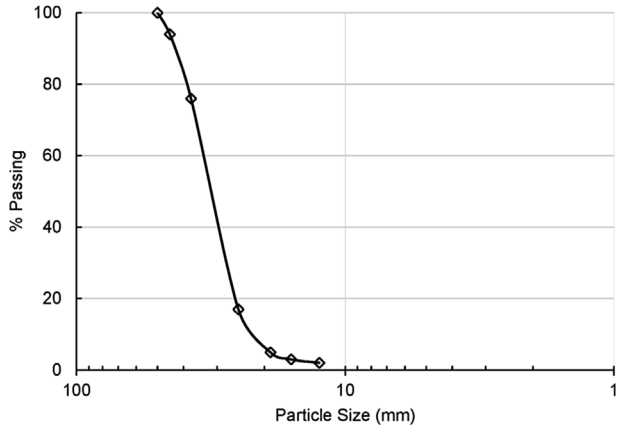

Fig. 3. Particle size distribution of ballast.

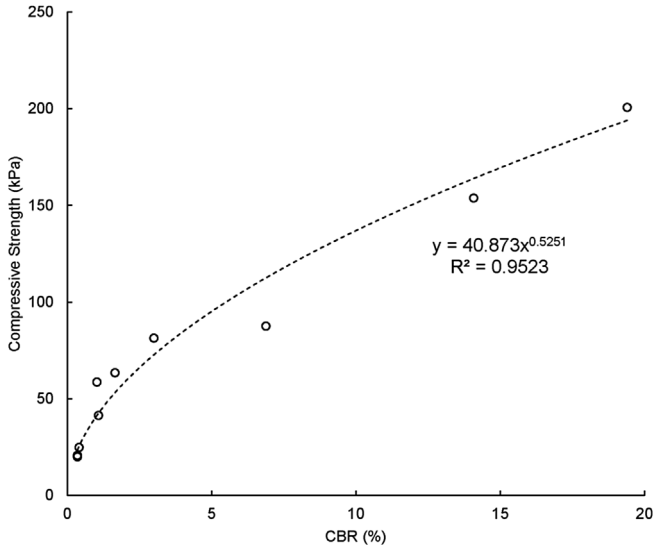

Fig. 4. CBR versus compressive strength of subgrade.

normal contact and friction coefficient of 0.4 (NAVFAC, 1986) for the tangential contact using the penalty friction algorithm. The geocell was modeled as an embedded part inside the ballast layer, representing an interface friction equivalent to the internal angle of friction, a behavior that has been observed in prior research studies (Biabani and Indraratna, 2015; Indraratna et al., 2011; Yang et al., 2010). Within geocells, confining behavior and apertures that accommodate increased roughness were assumed to provide a relatively rough interaction. The geotextile and ballast interface was modeled using the penalty friction algorithm, with hard normal contact and a friction coefficient of 2/

Table 1
Material properties.

Properties	Ballast	Subgrade	Geocell	Geotextile	Rail	Tie
Mass Density (kg/m^3)	1500	2162	950	950	8080	900
Elastic Modulus (MPa)	30	8.5	380	380	200,000	11,000
Poisson's Ratio	0.4	0.35	0.35	0.35	0.3	0.35
Internal Angle of Friction	45°	1°	–	–	–	–
Angle of Dilation	10°	1°	–	–	–	–

3tanϕ' for the tangential contact due to the relatively smoother surface of the geotextile. The geotextile was tied to the top of subgrade as the mass of ballast over the geotextile inhibited its movement, as observed in testing. The presence of ballast on top of the geotextile effectively roughened the relatively smooth surface of the geotextile caused by the localized asperities of the ballast on top.

Loading was applied in two stages. First, gravity was applied over a 100 s duration for stability under explicit conditions (i.e. to minimize residual kinetic energy in the model). Gravity was applied in separate step in order to simulate geostatic conditions right before the start of plate loading. This step allows the ballast to mobilize realistic frictional strength. Cyclic loading was applied in the next step as equivalent pressure load on top of a steel loading plate. The details of the plate loading sequence is shown in Fig. 2b. The loading was applied at a constant frequency of 1 Hz throughout. Semi-automatic mass scaling was used in order to reduce the time required for analysis with target time increment of 0.01 s for gravity and target time increment of 0.025 s for loading steps using non-uniformly scaled element mass to equal target time increment.

2.5. Comparison of experimental data and numerical results

The reinforced and unreinforced plate loading tests were modelled with same loading conditions and geometry. The loading in model was applied under load control conditions, similar to the actuator specifications of the experiment. The data from the model were recorded at approximately the same locations as the experiment for comparison.

Comparing the vertical displacement data from the unreinforced plate load test with the corresponding model, it is shown that the results match reasonably well. The model replicates the progressive displacement of the embankment with cyclic loading in Fig. 5a. The vertical stresses at the ballast-subgrade interface, although slightly underestimated, still capture the observed trends. The model captures the initial spike in pressure with increased loading and the subsequent redistribution of pressure with subsequent settlement Fig. 5c.

The reinforced plate loading test model captures the displacement behavior well. A slight divergence after 4000 cycles shown in Fig. 5b can be attributed to some difficulty achieving uniform and full compaction of ballast in the geocell during the experiment. The reinforced model also captures the trends in reduced difference in pressure between the center and 200 mm from center shown in Fig. 5d, resulting in a wider load distribution by geocell. The test data shows that interface pressure, particularly at the center and 200 mm from center is reduced by presence of the geocell system. Pressure cells were used to measure the pressures at the interface of the ballast and subgrade. The sensitive side of each pressure cell was faced down to ensure good contact between the sensitive area of the pressure cell and fine subgrade soil. All the pressure cells were buried into the subgrade with the top surface of the pressure cells flushed with the subgrade surface and leveled by a thin sand layer. The pressure cells were then covered with 25-mm thick stone chip (2.36 mm–4.75 mm size) to avoid the direct contact of ballast particles to the pressure cell surface. The settlement contours for the unreinforced plate loading test model at 6000 cycles are shown in Fig. 6 for a cross-section of the test box, presenting relatively localized displacement under very high loading (over 800 kPa). Fig. 7 shows the strain contours in the geocell for the reinforced plate load test. Intuitively, the cells near the loading plate exhibited the highest strains, realizing a maximum tensile strain of 0.96%. This indicates that the geocells were acting well within the elastic range. This observation was confirmed by the geocells exhibiting only superficial damage when exhumed following the laboratory experiments.

Although the agreement could certainly be improved by using more complex constitutive models, this study focused on using simple material parameters to capture realistic and complex geometry. The general agreement of the laboratory tests and three-dimensional numerical models were deemed satisfactory. Thus, the boundary conditions and materials properties were extrapolated to a parametric study, presenting opportunities to expand beyond the experimental limitations to practical railroad geometry and loading.

2.6. Parametric study

Using the calibrated models obtained, a parametric study was conducted in order to characterize the effectiveness of geocell confinement for railway embankments crossing soft subgrade materials. Within this parametric analysis, embankment geometry, subgrade CBR, and geocell configuration were altered to highlight important design aspects. During these simulations, relevant data including settlement, lateral displacements, and geocell strains were extracted during 100,000 cycles of train wheel loading.

2.7. Geometry

A typical ballast railway embankment consisting of ballast 0.3 m in depth that was placed on a weak overlaying subgrade was selected as a baseline numerical model. This section was placed on top of 2 m deep subgrade, deep enough to minimize stress boundary effects, and kept at 5 m in length. The side slope of the ballast embankment was kept constant at 2(H):1(V). The tie track arrangement along with an exploded view of the modeled embankments is shown in Fig. 8. For comparison, similar models with a ballast section 0.45 m and 0.6 m in depth and with 0.3 m ballast section embedded flush in the subgrade were modelled as well. For all models, the track and tie arrangement was kept the same. For these models, there were different reinforcement conditions, detailed in Table 2, and the respective geometric representation are shown in Fig. 9. For “Reinforced 0.15 m below subgrade” case, 0.15 m thick layer of subgrade underneath the ballast embankment was replaced with ballast and reinforced with geocell. Due to fouling, ballast are required to be cleaned regularly using specialized heavy equipment. For this purpose, it is unlikely that geocell can be placed less than 0.15 m below the ties. However, for locations with frequent loss of track geometry, use of geocells can be a viable solution when placed in the lower portions of the embankment.

Taking advantage of the symmetry of the section, only half of the embankment was modeled, enabling “mirroring” of the conditions of a full embankment. Geocell arrangement was symmetric on both half and lateral movement of the geocell elements was constrained at the plane of symmetry in order to simulate anchorage form the missing half. The section was modeled to accommodate three ties in width – considered to be adequately representative of the load-bearing tributary area for rail wheel loading (Leshchinsky and Ling, 2013b). The details of the tie and track arrangement in the ballast are shown in Fig. 8a and b. The cross section of the tie was 0.23 m × 0.178 m and 1.3 m long (for the symmetrical half modelled) supporting a 0.6 kN/m rail (136 lb/yard AREMA rail). The center line of the track was 0.718 m from the symmetry line of the embankment. Details of 0.6 m embankment model reinforced to full width and reinforced 0.15 m below subgrade are shown in Fig. 8c and d, respectively. The distance from the end of tie to start of side slope (shoulder) was fixed for all models at 0.3 m.

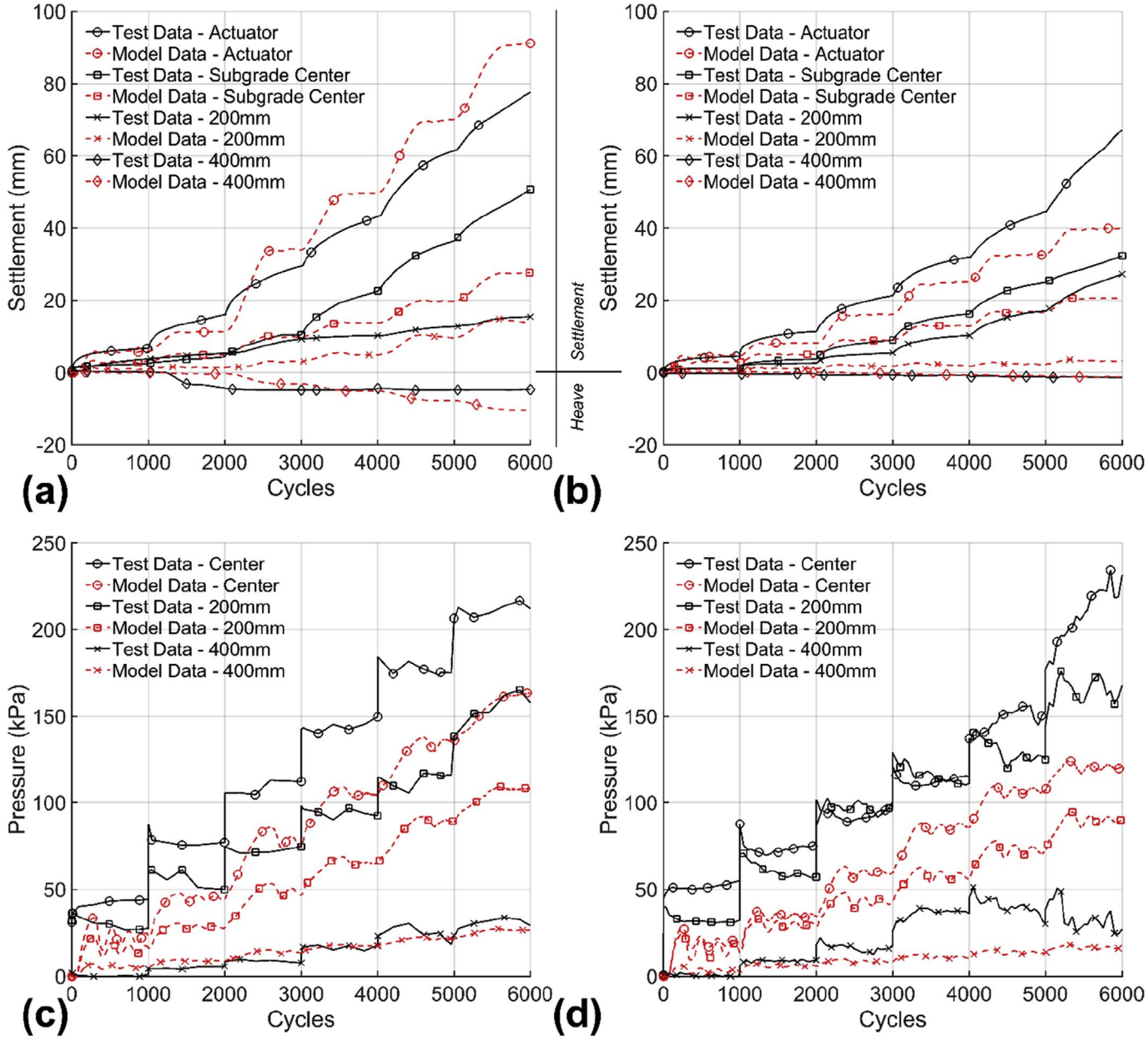

Fig. 5. Comparison of FE model outputs with experimental data for (a) unreinforced model displacements, (b) reinforced model displacements, (c) unreinforced model interface pressure, and (d) reinforced model interface pressure.

For each case, the subgrade was simulated using four different CBR values, using representative unconfined compressive strengths of the subgrade shown in Table 3. The subgrade strength was limited to a 3% CBR (q_u = 75 kPa) to observe maximum efficacy of the reinforcement. On weak subgrades, the effectiveness of mechanical reinforcement in reducing settlement decreases significantly beyond 3% CBR (Montanelli et al., 1997).

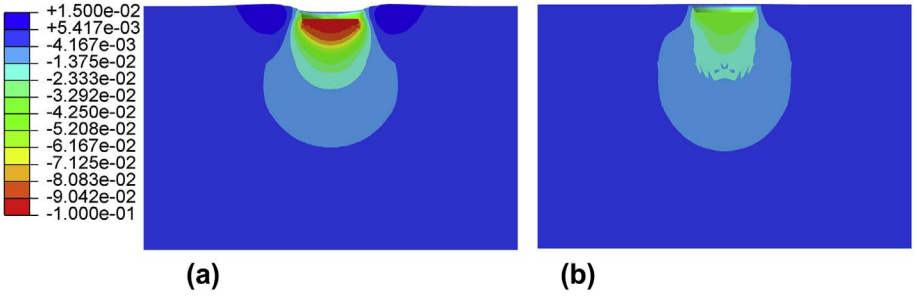

Fig. 6. Settlement (m) contours at 6000 cycles for (a) Unreinforced and (b) Reinforced models.

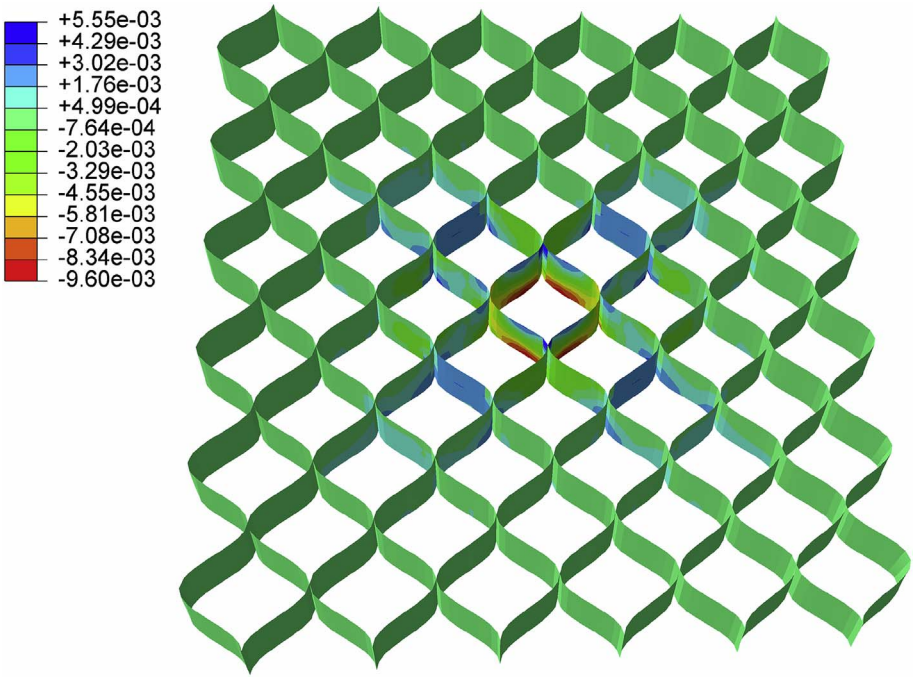

Fig. 7. Reinforced box model strain in geocell (tension - negative).

2.8. Materials

The calibrated material properties and material models used for the parametric study are summarized in Table 1. The rail and tie had significantly higher stiffness than the ballast and subgrade and were not expected to yield, thus were also modeled as linear elastic material. The material properties of ties are representative of treated oak ties (Frostick et al., 2014).

2.9. Mesh and boundary conditions

Only half of the embankment was modelled, taking advantage of the symmetry. The ballast, subgrade, loading plate, rail and ties were meshed using C3D8R (brick) elements. Geocells and geotextiles were

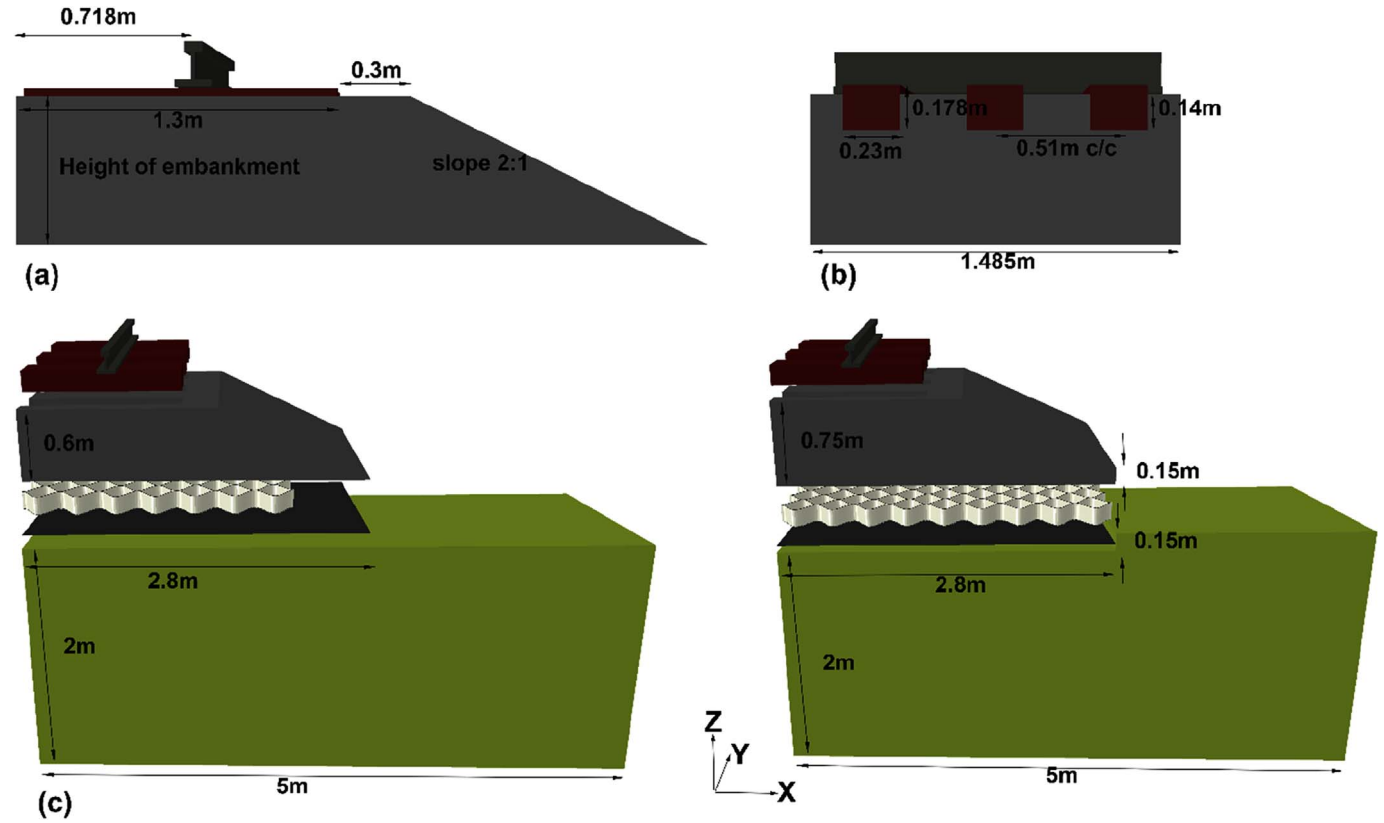

Fig. 8. Model schematics for parametric study: Tie/track arrangement (a) Along the track (b) Parallel to the track (c) Exploded view of 0.6 m embankment, and (d) Exploded view of 0.6 m embankment with geocell 0.15 m below subgrade level.

Table 2
Reinforcement conditions and representations for parametric study.

Reinforcement Conditions	0.6 m ballast embankment	0.45 m ballast embankment	0.3 m ballast embankment
Unreinforced	0.6U	0.45U	0.3U
Reinforced below tie	0.6R T	0.45R T	0.3R T
Reinforced below shoulder	0.6R S	0.45R S	0.3R S
Reinforced to full width	0.6R FW	0.45R FW	0.3R FW
Reinforced 0.15 m above subgrade	0.6R HI	0.45R HI	–
Reinforced with 2 layers of geocell	0.6R TWO	0.45R TWO	–
Reinforced 0.15 m below subgrade	0.6R LO	0.45R LO	0.3R LO

meshed using M3D4R (membrane) elements. The average size of ballast, rail and tie elements was 20 mm. Smaller size ballast elements were used in order to focus computational effort on the ballast, where the most deformation was expected. The interface between the ballast and tie surfaces were modelled with hard normal contact and a penalty friction algorithm. The frictional coefficients used in this relationship were 0.4 between the bottom of the tie and the ballast and 0.1 for vertical sides of the ties and ballast in order to account for relatively low confinement and reduced interaction (Le Pen, 2008). As in the experimental testing, the geocell was modeled as embedded part inside the ballast layer. The x direction is perpendicular to the length of track (left positive), y direction is along the length of track (inward positive) and z direction is vertical (upward positive). For boundary conditions, the lateral displacements in outer edges of the z-y planes were constrained in x-direction and outer edges of z-x planes were constrained in y-direction. The bottom of the subgrade was restricted from any displacements. These boundary conditions preserved the symmetry of the model in z-y plane and also the plane strain condition was maintained in the longitudinal direction of the railroad alignment.

2.10. Loading

The stepwise nature of loading used in the parametric study was similar to that of the simulated comparisons to the laboratory experiments, with a loading step following the gravity step. For this parametric study, the same haversine shape shown in Fig. 2a was used, but the frequency of the load was changed to 16 Hz to represent the corresponding average train speed of 120 km/h (Indraratna et al., 2010). For the physical test loading equivalent to a light train was used. For the parametric analysis, train wheel load of 200 kN, representative of the most severe loading case from rail freight (Esveld, 2001; Selig and Waters, 1994) was used. These simulations were run for 100,000 cycles and data was extracted every 10 virtual seconds (160 cycles) in order to observe the trends in fine detail while avoiding drastically longer simulation time and data storage issues.

3. Results and discussion

From all the models used in the parametric study, the track settlement, subgrade settlement, pressure at the interface of ballast and subgrade, strains in geocells and the change in geometry (heave) at the slope of the embankments were measured.

Vertical settlement of the track geometry, particularly differential settlement, can compromise railroad function. Geocell reinforcement may present an effective means of neutralizing soft spots via localized confinement at the subgrade-ballast interface. To illustrate these effects, track settlement is presented graphically for 100,000 cycles of freight loading in Fig. 10. The results demonstrate resilient behavior with cyclic loading – that is, there is more initial settlement with load cycling followed by reduced residual displacements after many cycles. For unreinforced models, the slope of progressive cyclic settlement was steeper than the reinforced model, suggesting less resilience under

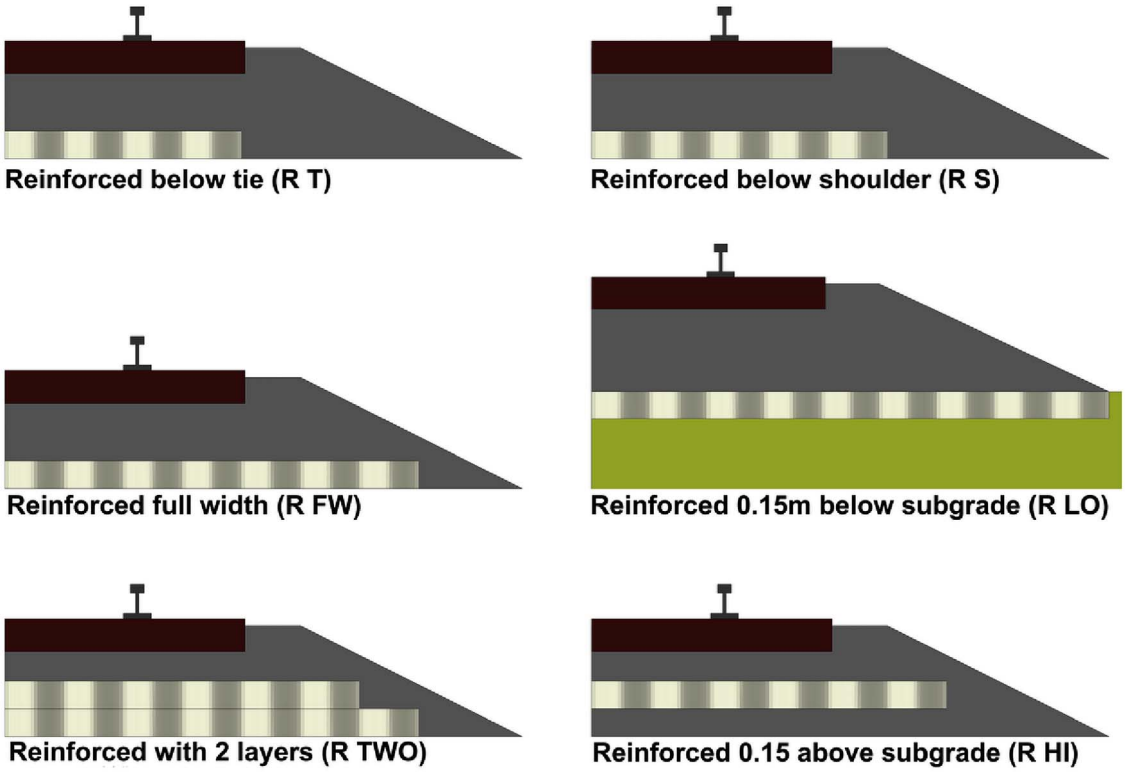

Fig. 9. Geocell arrangement for parametric study.

Table 3
Unconfined compressive strengths for different CBR values used in simulated subgrades.

CBR (%)	Unconfined compressive strengths (kPa)
0.5	30
1	40
2	60
3	75

cyclic loading. For all subgrade strengths, the reduction in settlement due to geocell reinforcement is significant, although less pronounced for higher subgrade strengths. On average, there is an approximately 30% decrease in track settlement due to geocell confinement. More competent subgrades undergo less lateral squeeze and heave, thus exhibiting lower unreinforced settlement. And with the addition of geocell reinforcement, lateral heave of ballast is reduced and thus the track settlement is further decreased. The wider distribution of stresses enables a larger region of the subgrade to mobilize shear strength, resulting in inhibited track settlement.

Enhanced geocell reinforcement can be achieved through strategic placement of geocell confinement in the embankment material. Placing two layers of geocell on top of each other on the subgrade ballast interface results in least track settlement (Fig. 11). When using a single layer of geocell, placing the layer closer to the ties (higher in the ballast embankment) results in better performance. In the case of 0.6 m embankment on a 0.5% CBR subgrade, placing the geocells 0.15 m (height of one layer of geocell) higher results in additional 5% decrease in track settlement. It also demonstrates a more even distribution of subgrade pressure and reduces the lateral heave on the crest of the embankment, consequently reducing settlement. The placement of geocell closer to the ties demonstrates an ability to mobilize increased confinement behavior. This confinement reduces the settlement in ballast layer and the pressure transferred to subgrade, results in lower permanent deformation of the soft subgrade. Although placing the geocells higher in the embankment yields better performance, the geocells cannot be installed closer than 0.15 m to the tie as it can cause obstruction to the regular maintenance of the railroad.

Increasing geocell coverage underneath the ties demonstrated reduced settlement, however little added benefit was realized when it extended far beyond the shoulder. This is because the maximum observed stress on the subgrade occurred at the end of ties with little stress transfer occurring beyond the toe of the embankment. Consequently, the transfer of larger magnitudes of vertical stress from the ties increased confinement and mobilized strains in the subsurface geocell, but this benefit was muted outside the stress bulbs of the ties. This

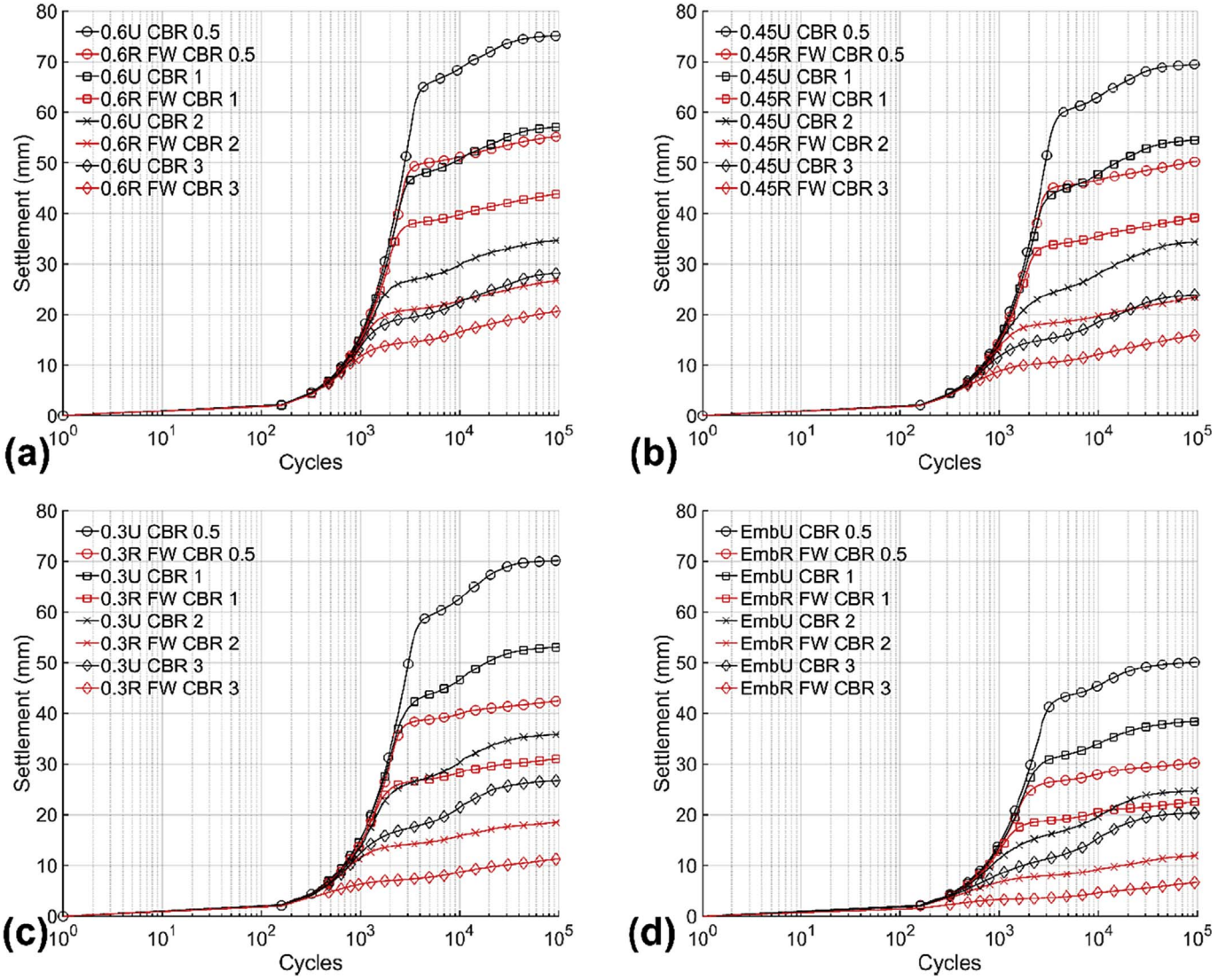

Fig. 10. Track settlement vs cycles of loading – comparison of reinforced (full width) and unreinforced models for (a) 0.6 m embankment, (b) 0.45 m embankment, (c) 0.3 m embankment, and (d) embedded embankment.

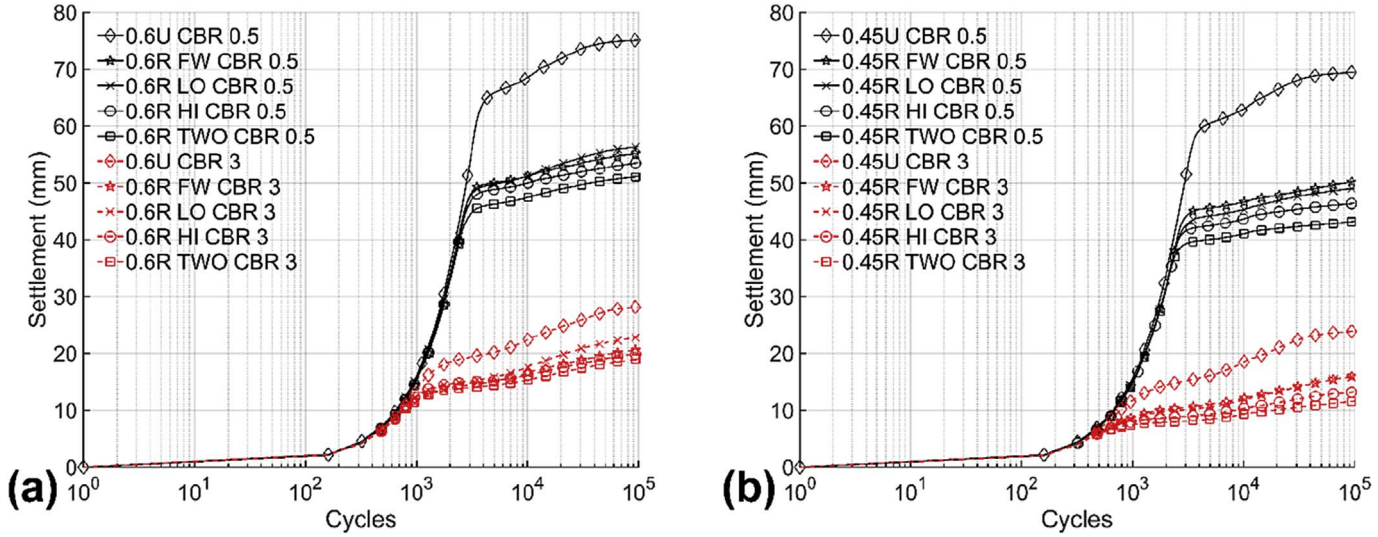

Fig. 11. Track settlement vs. cycles – comparison of reinforcement location for (a) 0.6 m embankment with CBR 0.5% and 3%, (b) 0.45 m embankment with CBR 0.5% and 3%.

implies that addition of reinforcement beyond the shoulder may aid in wider stress distribution of under the end of ties but does not result in significant decrease in track settlement.

Maximum tensile strains measured in the geocells were in the elastic range for typical geosynthetic materials (Table 4) for all of the cases (Yang, 2010). The maximum value of tensile strain was 1.57%, measured over a very weak subgrade (CBR = 0.5%) when the geocell was placed close to the tie. Strain in geocell increased with proximity to the tie. With increased stress localization closer to the load-bearing ties, the geocell exhibits higher strains to confine its infill. At lower depths, the load is dissipated, in turn reducing the amount of strain mobilized. For a given reinforcement configuration, geocell strains increased with weaker subgrades. Under a similar loading condition, weaker subgrades displace more. Such a behavior is detrimental, but simultaneously mobilizes the mattress, reinforcing effects of the geocell confinement, effectively reducing concentrated subgrade stresses and deformation. For a given subgrade strength and embankment configuration, the maximum tensile strain in the geocell did not change significantly with geocell coverage. However, when two layers of geocell were used, the overall strain was reduced, but was found to be higher in the upper geocell layer. Use of more ballast also reduced strains, likely due to the decreased mobilization of geocell confinement. This demonstrates that the benefit of geocell is most pronounced when less ballast is present. The maximum tensile strains in geocell was located underneath the end of ties and shoulder (Fig. 12). This band tended to be one or two cells in width. Due to bending behavior of the geocell mattress, tensile strain was mostly localized at the bottom corners of the geocells. This observation is important for practical applications as insufficient seam strength could result in rupture, as observed in geocell reinforcement in Leshchinsky and Ling (2013a).

The confining behavior of geocell in flexure reduces interface pressures exhibited at the ballast subgrade interface. Higher stresses occurred at the subgrade underneath unreinforced embankments, notably beneath the ties (Fig. 13). However, use of geocell reduced the stresses more uniformly. This uniform distribution of stress is beneficial towards maintaining track geometry through two mechanisms: (1) distributing track loads to larger area of weak subgrade, resulting in less plastic deformation, and (2) arrested heave of the unconfined ballast embankment.

The ballast-subgrade interface pressure under loading and the

Table 4
Maximum tensile strains in geocell.

Maximum tensile strain in geocell (%)												
Reinforcement Conditions	0.6 m ballast embankment				0.45 m ballast embankment				0.3 m ballast embankment			
Subgrade CBR (%)	0.5	1	2	3	0.5	1	2	3	0.5	1	2	3
Geocell below tie	0.62	0.49	0.36	0.3	0.76	0.58	0.65	0.47	1.08	0.87	0.59	0.57
Geocell below shoulder	0.68	0.52	0.38	0.31	0.81	0.67	0.52	0.44	-	-	-	-
Geocell below full width	0.69	0.53	0.38	0.31	0.85	0.7	0.5	0.45	1.25	0.96	1.5	0.73
Geocell 0.15m above subgrade	0.88	0.76	0.61	0.53	1.57	1.42	1.16	1.07	-	-	-	-
2 layers of geocell (top layer)	0.59	0.48	0.41	0.36	1.13	0.65	0.7	0.91	-	-	-	-
2 layers of geocell (bottom layer)	0.69	0.54	0.38	0.29	0.73	0.62	0.41	0.36	-	-	-	-
Geocell 0.15m below subgrade	0.7	0.66	0.47	0.3	0.62	0.5	0.45	0.28	0.81	0.69	0.48	0.41

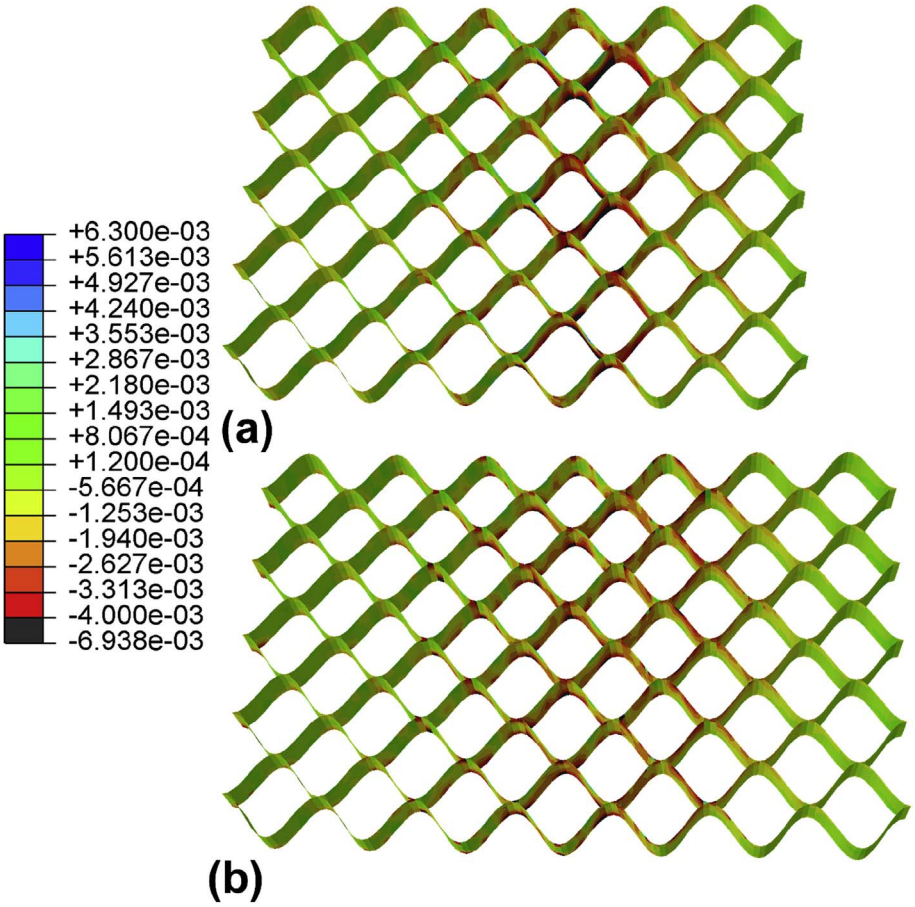

Fig. 12. Geocell strain at 100,000 cycles for (a) 0.45 m embankment on CBR 0.5% subgrade and (b) 0.6 m embankment on CBR 0.5% subgrade (tension - negative).

influence of geocell on this behavior are shown in Fig. 14. The interface pressure acting on the subgrade did not change significantly based on the strength of the subgrade. A "peak" pressure occurred at the onset of loading, attributed to the onset of initial plastic deformation of virgin subgrade material. As the material deforms, it changes the stress-transfer mechanism and thereby decreases the maximum stress that occurs. Use of geocell reduced this initial peak. For a 0.6 m embankment over a 0.5% and 1% CBR subgrades, geocell reinforcement reduced the interface pressure (post peak) from 88 kPa to 52 kPa (40%) and 88 kPa–55 kPa (38%), respectively.

The location of geocell reinforcement did not change the ballast-subgrade interface pressures significantly with the exception of two cases: a reinforced embankment with two layers of geocell and when the geocell was embedded in ballast 0.15 m beneath the ground surface. With two layers of geocell, the decrease in interface pressure was the largest. Due to the combined confining effect of the two layers, the stress transferred from the track was redistributed significantly by the time it reached the subgrade as the embankment demonstrated composite behavior. In the case of the geocell reinforcement placed 0.15 m below grade, the decrease in interface pressure was the lowest as the

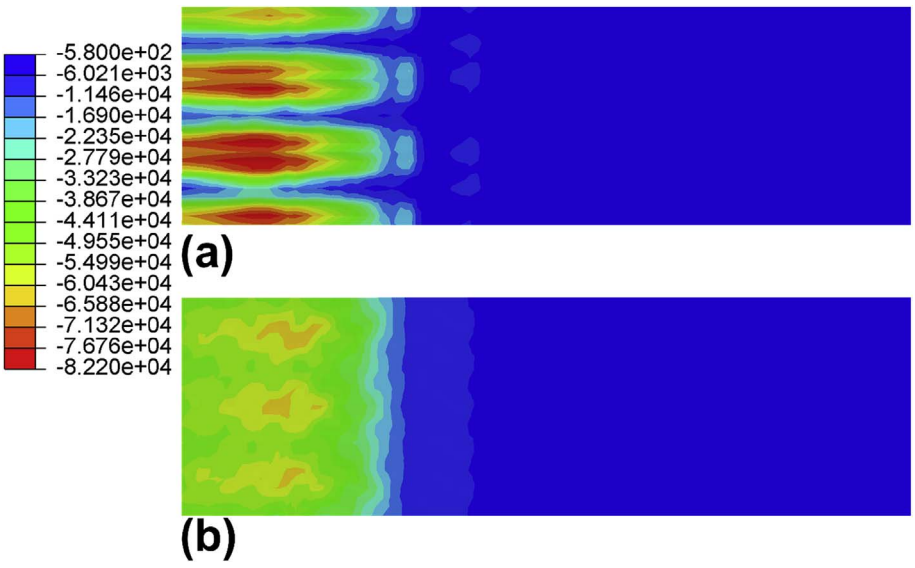

Fig. 13. Interface pressure (Pa) on the subgrade at the end of 100,000 cycles for the (a) Unreinforced 0.45 m embankment and (b) Reinforced (full width) 0.45 m embankment.

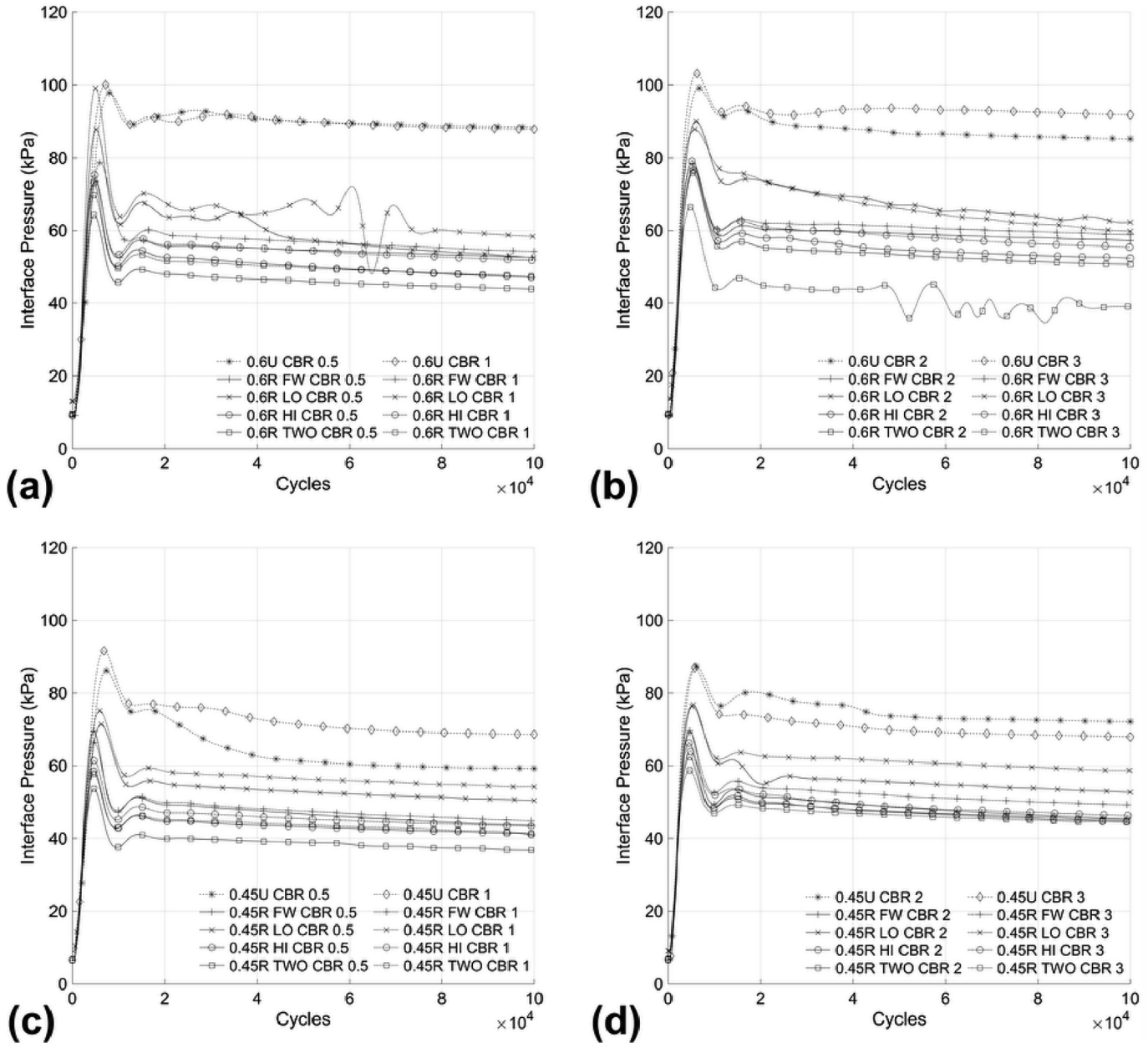

Fig. 14. Interface pressure vs. cycles – comparison of reinforcement location for (a) 0.6 m embankment with CBR 0.5% and 1%, (b) 0.6 m embankment with CBR 2% and 3%, (c) 0.45 m embankment with CBR 0.5% and 1% and (d) 0.45 m embankment with CBR 2% and 3%.

geocell layer was located furthest away from the ties and offered the least confinement to the ballast.

Use of geocell reinforcement reduced settlement of ballasted railway embankments. With the additional confinement offered by geocell and wider distribution of pressure, the stress acting on subgrade was reduced and decreased deformation (Fig. 15). For example, when considering an embankment 0.6 m in height on a very weak subgrade (CBR = 0.5%) with full-width geocell reinforcement, the subgrade settlement was reduced by nearly 26% (75 mm–55 mm) and for CBR 1% subgrade, the reduction was 26% (56 mm–43 mm). With stronger subgrades, the percentage reduction in subgrade settlement was less than of a weaker subgrade. Even for the strongest subgrade analyzed (CBR = 3%), there was reduction in settlement of nearly 22% (31 mm–24 mm). The reduction in settlement was not sensitive to the location of geocells with the exception of when two layers of geocell were used. When two layers of geocell were used as reinforcement, there was a greater reduction in settlement. For example, for a 0.6 m tall embankment on a 0.5% CBR subgrade with two layers of geocell reinforcement, the subgrade settlement was reduced by 33% (75 mm–50 mm) in comparison to the unreinforced case. From the study, it was also observed that reinforcement coverage beyond the shoulder did not significantly reduce settlement. As expected from the strain data in geocell, strains were limited outside the shoulder of the embankment, having little influence on settlement.

Use of geocell reinforcement increased the number of load cycles required to attain the same amount of subgrade settlement compared to unreinforced case. For example, when considering an embankment 0.6 m in height on a very weak subgrade (CBR = 0.5%), the subgrade settlement of 50 mm was attained at the end of 4000 loading cycles when unreinforced whereas with two layers of geocell reinforcement, the same amount of subgrade settlement was attained at the end of 30,720 loading cycles. For the same embankment, the subgrade settlement of 52 mm was attained at the end of 4160 loading cycles when unreinforced whereas with full-width geocell reinforcement, the same

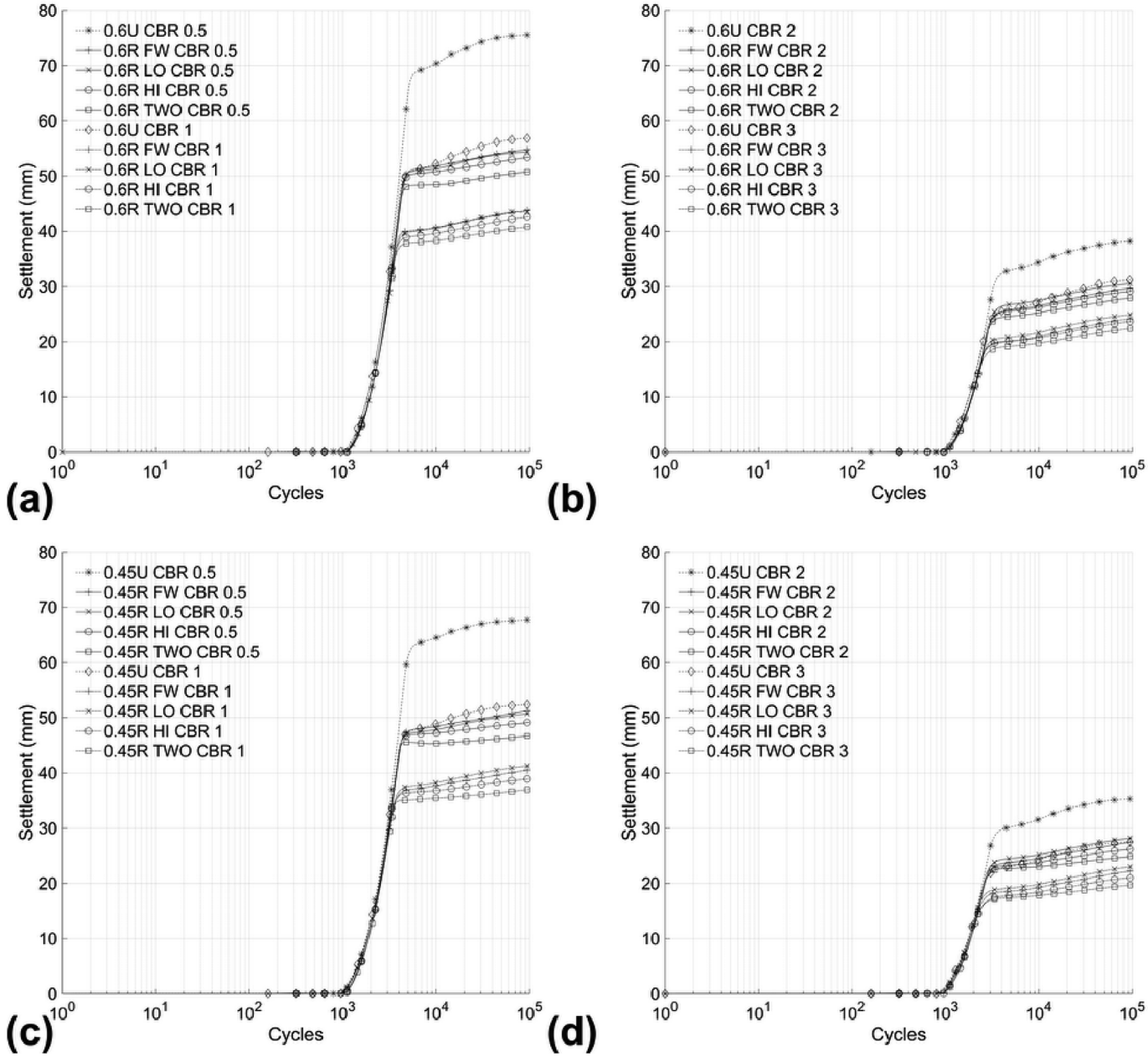

Fig. 15. Subgrade settlement vs. cycles – comparison of reinforcement location for (a) 0.6 m embankment with CBR 0.5 and 1, (b) 0.6 m embankment with CBR 2 and 3, (c) 0.45 m embankment with CBR 0.5 and 1 and a (d) 0.45 m embankment with CBR 2 and 3.

amount of subgrade settlement was attained at the end of 11,360 loading cycles.

Track geometry, including the side slopes of the railway embankment degraded from the lateral displacement of ballast over repeated loading cycles. Geocell may arrest this heave behavior by confining the ballast material from lateral movement (crest displacements shown in Table 5). It was observed that the geocell reinforcement (full width) decreased the lateral displacement of the embankment toe overlying a weak subgrade (CBR = 0.5%) by around 20% (40.2 mm–32 mm) for a 0.6 m tall embankment. For the same case, the lateral displacement of crest of side slope was reduced by around 73% (19.1 mm–5 mm). With more competent subgrades, the decrease in lateral displacement is reduced. It was also observed that the amount of lateral displacement increased with increased embankment depth. From the study it was also observed that geocell decreased the lateral displacement of ballast laying on top of the reinforced layers and less effectively below the reinforced layers. It is important to note that the geocell reinforcement did not extend to the toe of the embankments. If any portion of a cell protruded outside of the side slope, length of geocell reinforcement was decreased in order to contain only fully embedded cells. This criterion was implemented in order to assess the reinforced and unreinforced cases without changing the geometry and for the ease of modelling.

The change in side-slope geometry at the end of 100,000 cycles for a 0.6 m embankment on a very weak (CBR = 0.5%) subgrade is shown in Fig. 16a. These results demonstrate that two layers of geocell reinforcement offer the maximum reduction in lateral displacement. For a single layer of reinforcement, placing the reinforcement 0.15 m above subgrade provides the maximum reduction of lateral deformation at the crest. However, the maximum reduction of lateral deformation of the toe can be achieved by placing a full width reinforcement on top of the subgrade. This is due to the lack of geocell confinement to the edge of the side slope. Considering all the cases, geocell reinforcement offers improved retention of embankment geometry for railway embankments.

Table 5
Lateral displacement of ballast at crest of side slope of embankment.

Lateral displacement at the end of 100,000 cycles at crest of side slope (mm) (outward positive)												
Reinforcement Conditions	0.6m ballast embankment				0.45m ballast embankment				0.3m ballast embankment			
Subgrade CBR (%)	0.5	1	2	3	0.5	1	2	3	0.5	1	2	3
Unreinforced	19.1	20.1	16.1	15.4	16	15.7	13.9	13.9	13.6	12.4	9.6	8.1
Geocell below tie	7.2	9.3	10.8	10.7	4.8	7.5	8.9	9.3	2.6	2.8	7.1	6.3
Geocell below shoulder	4.8	7.9	9.5	8.6	1.9	4.5	7.5	7.9	-	-	-	-
Geocell below full width	5	7.7	8.9	9.2	0.6	3.8	6	7.3	-3.1	1.7	7	4.2
Geocell 0.15m above subgrade	0.7	4.1	6.7	6.8	-2.2	0.8	3.3	4.2	-	-	-	-
2 layers of geocell	-1	1.8	4.6	5.7	-5.5	-3.1	1.1	1	-	-	-	-
Geocell 0.15m below subgrade	4.9	8.3	9.1	10	2.6	5.5	7.1	7.9	-0.5	2.7	4.8	5.9

The lateral displacement of the embankment side-slopes increased with an increasing number of load cycles (Fig. 16b). The reinforced embankment maintained the original slope geometry better in comparison to the unreinforced case. The difference in lateral displacement of the side slope between the reinforced and unreinforced model increased with increasing loading cycles. Comparing the lateral displacement of side slope in 10,000th loading cycle with 100,000th loading cycle, it is evident that the reinforced embankment undergoes significantly less lateral displacement compared to the unreinforced case. Further, the reduction in lateral displacement of ballast embankment due to geocell confinement on a very weak subgrade (CBR = 0.5%) is shown in Fig. 17.

4. Conclusions

A series of large-scale experimental plate loading tests demonstrated that use of geocell confinement for ballast overlying weak subgrade materials improved performance through reduced settlement and subgrade pressures. Calibrated numerical simulations of the physical experiments were created using three-dimensional finite element analyses, demonstrating general agreement with experimental data. Upon this agreement, a parametric study was performed using realistic railway embankment geometry and loading, enabling observation of geocell configuration, embankment geometry and subgrade properties on railway embankment performance. Some of the conclusions inferred form the study are as follows:

1. Geocell confinement reduced the settlement of the track for all observed subgrade strengths, particularly weak subgrades. Greater subgrade strengths reduced the benefit of geocell reinforcement for additional confinement. The rate of continuous settlement due to cyclic loading was reduced through use of geocell reinforcement.
2. The use of geocell confinement was very effective in redistributing the vertical stresses on the subgrade, resulting in larger areas of subgrade mobilizing shear strength and reducing plastic deformations. Improved subgrade performance from geocell confinement

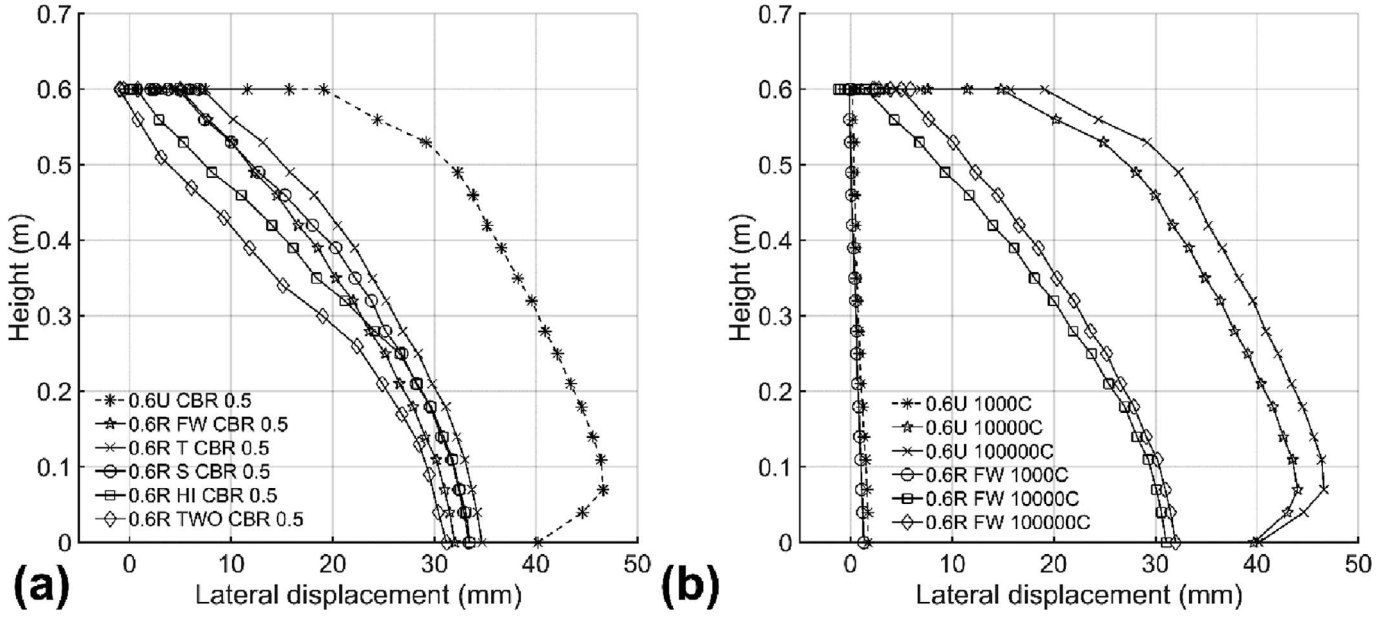

Fig. 16. Change in geometry – side slope: (a) 0.6 m embankment at 100,000 cycles on CBR 0.5% subgrade, and (b) 0.6 m embankment on CBR 0.5% subgrade at different load cycles.

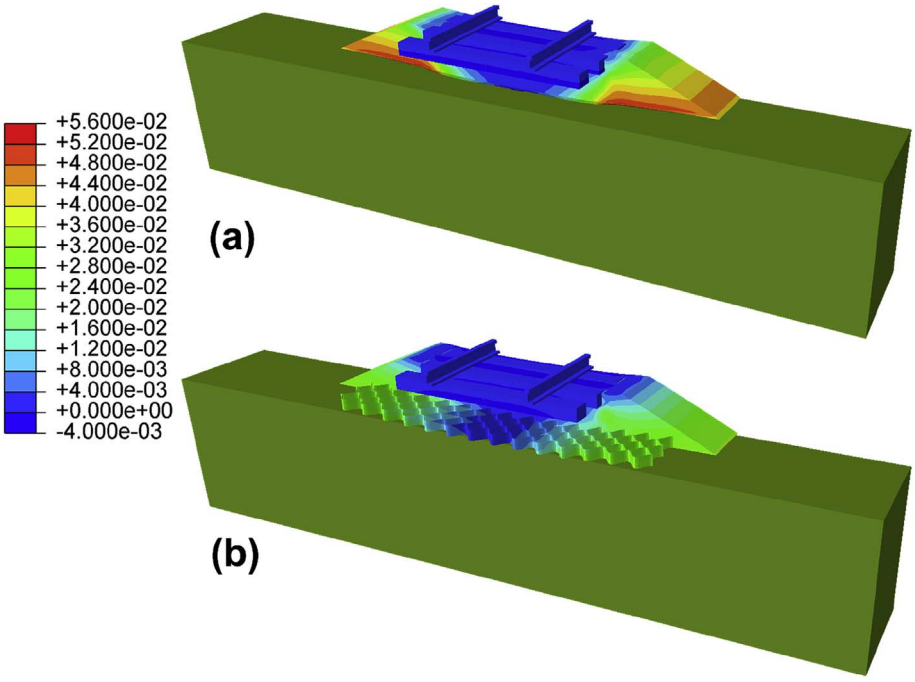

Fig. 17. Lateral displacement (m) of the ballast embankment at the end of 100,000 cycles for (a) Unreinforced 0.6 m embankment and (b) Reinforced 0.6 m embankment on 0.5% CBR subgrade (positive values indicate outward displacement).

occurring from redistribution of vertical stresses did not vary significantly for the observed range of subgrade strengths. Finally, the redistribution of stresses occurred in the initial cycles for all cases, exhibiting an initial peak in ballast-subgrade pressures followed by relatively stead pressures. Geocell muted this behavior to some level, mainly due to the reduced pressures observed.

3. For the loading conditions used in the analyses, the strains in geocell were low and within the elastic range for typical geosynthetic materials. The maximum tensile strains were localized at the bottom corners of the cells, showing the importance of adequately durable seams. For the plate loading model, tensile strain localized under the loading plate at bottom corners and for the railway embankment models, it was localized directly under the end of ties forming a band one to two cells in width along the length of track.
4. Subgrade settlement was significantly reduced from use of geocell confinement. The more uniformly distributed vertical stresses effectively reduced the vertical settlement of the subgrade observed due to an arrest of subgrade plastic deformation. With reduced subgrade settlement, geocell confinement helped to preserve the geometry of the track.
5. Lateral displacements along the side slopes of the railroad embankment were greatly reduced through use of geocell confinement. Reduction in lateral displacement was significantly higher in weaker subgrades. The confinement offered by cellular geometry of the geocell likely prevents the lateral heave of the material along with the mattress effect stemming from the confinement of the granular ballast.

Use of geocell reinforcement to improve the settlement performance of the track may be instrumental in increasing track maintenance cycles, enhancing track capacity and preventing differential settlement over localized areas of soft soil. Future work could look at further cyclic loading, different track geometries, alternative loading conditions, and the degradation of ballast with geocell confinement.

Acknowledgments

The authors gratefully acknowledge Presto GeoSystems® for the support of this study. The plate loading test was carried out at The University of Kansas (KU). The authors would like to thank the geotechnical engineering group and students at the geotechnical laboratory at KU for their help.

References

Ahlf, R.E., 1975. M/W Costs: how they are affected by car weights and the track structure. Railw. Track Struct. 71 (3), 34.
Bathurst, R.J., Karpurapu, R., 1993. Large-scale triaxial compression testing of geocell-reinforced granular soils. Geotechnical Test. J. 16 (3), 296–303.
Biabani, M.M., Indraratna, B., 2015. An evaluation of the interface behaviour of rail subballast stabilised with geogrids and geomembranes. Geotext. Geomembranes 43 (3), 240–249.
Biabani, M.M., Indraratna, B., Ngo, N.T., 2016b. Modelling of geocell-reinforced subballast subjected to cyclic loading. Geotext. Geomembranes 44 (4), 489–503.
Biabani, M.M., Ngo, N.T., Indraratna, B., 2016a. Performance evaluation of railway subballast stabilised with geocell based on pull-out testing. Geotext. Geomembranes 44 (4), 579–591.
Biswas, A., Krishna, A.M., 2017. Behavior of geocell-geogrid reinforced foundations on clay subgrades of varying strengths. Int. J. Phys. Model. Geotechnics 1–50.
Esveld, C., 2001. Modern Railway Track. MRT-productions Zaltbommel, The Netherlands.
Frostick, L.E., Thomas, R.E., Johnson, M.F., Rice, S.P., McLelland, S.J., 2014. Users Guide to Ecohydraulic Modelling and Experimentation: Experience of the Ecohydraulic Research Team (PISCES) of the HYDRALAB Network. CRC Press.
Giroud, J.P., Han, J., 2004. Design method for geogrid-reinforced unpaved roads. II. Calibration and applications. J. Geotech. Geoenviron. Eng. 130 (8), 787–797.
Han, J., Pokharel, S.K., Yang, X., Manandhar, C., Leshchinsky, D., Halahmi, I., Parsons, R.L., 2011. Performance of geocell-reinforced RAP bases over weak subgrade under full-scale moving wheel loads. J. Mater. Civ. Eng. 23 (11), 1525–1534.
Han, J., Yang, X.M., Leshchinsky, D., Parsons, R.L., Rosen, A., 2008. Numerical analysis for mechanisms of a geocell-reinforced base under a vertical load. Geosynth. Civ. Environ. Eng. Shanghai, China 741–746.
Hegde, A., 2017. Geocell reinforced foundation beds-past findings, present trends and future prospects: a state-of-the-art review. Constr. Build. Mater. 154, 658–674.
Hegde, A., Sitharam, T.G., 2015. 3-Dimensional numerical modelling of geocell reinforced sand beds. Geotext. Geomembranes 43 (2), 171–181.
Hibbitt, Karlsson, Sorensen Inc, 2007. ABAQUS Documentation. Dassault Systèmes, Providence, RI, USA.
Indraratna, B., Biabani, M.M., Nimbalkar, S., 2015. Behavior of geocell-reinforced subballast subjected to cyclic loading in plane-strain condition. J. Geotechnical Geoenvironmental Eng. 141 (1), 04014081.
Indraratna, B., Hussaini, S.K.K., Vinod, J.S., 2011. On the Shear Behavior of Ballast-Geosynthetic Interfaces.
Indraratna, B., Ionescu, D., Christie, H., 1998. Shear behavior of railway ballast based on large-scale triaxial tests. J. Geotechnical Geoenvironmental Eng. 124 (5), 439–449.
Indraratna, B., Nimbalkar, S., 2013. Stress-strain degradation response of railway ballast stabilized with geosynthetics. J. Geotechnical Geoenvironmental Eng. 139 (5), 684–700.
Indraratna, B., Nimbalkar, S., Christie, D., Rujikiatkamjorn, C., Vinod, J., 2010. Field assessment of the performance of a ballasted rail track with and without

geosynthetics. J. Geotechnical Geoenvironmental Eng. 136 (7), 907–917.
Koerner, R.M., 2012. Designing with Geosynthetics. Xlibris Corporation.
Lackenby, J., Indraratna, B., McDowell, G., Christie, D., 2007. Effect of confining pressure on ballast degradation and deformation under cyclic triaxial loading. Géotechnique 57 (6), 527–536.
Le Pen, L., 2008. Track Behaviour: the Importance of the Sleeper to Ballast Interface. University of Southampton.
Leshchinsky, B.A., 2011. Enhancing ballast performance using geocell confinement. Geo-Frontiers 2011 Adv. Geotechnical Eng. 4693–4702.
Leshchinsky, B., Ling, H., 2013a. Effects of geocell confinement on strength and deformation behavior of gravel. J. Geotechnical Geoenvironmental Eng. 139 (2), 340–352.
Leshchinsky, B., Ling, H.I., 2013b. Numerical modeling of behavior of railway ballasted structure with geocell confinement. Geotext. Geomembranes 36, 33–43.
Montanelli, F., Zhao, A., Rimoldi, P., 1997. Geosynthetic-reinforced pavement system: testing and design. In: Proceeding of Geosynthetics, Long Beach, California, pp. 619–632.
NAVFAC, M., 1986. Foundations and Earth structures. Des. Man. 7, 63.
Pokharel, S.K., Han, J., Leshchinsky, D., Parsons, R.L., 2017. Experimental evaluation of geocell-reinforced bases under repeated loading. Int. J. Pavement Res. Technol. http://dx.doi.org/10.1016/j.ijprt.2017.03.007. (in press).
Rajagopal, K., Krishnaswamy, N.R., Latha, G.M., 1999. Behaviour of sand confined with single and multiple geocells. Geotext. Geomembranes 17 (3), 171–184.
Raymond, G.P., 2001. Failure and reconstruction of a gantry crane ballasted track. Can. Geotech. J. 38 (3), 507–529.
Selig, E.T., Waters, J.M., 1994. Track Geotechnology and Substructure Management. Thomas Telford.
Skempton, A.W., 1951. The bearing capacity of clays. Build. Res. Congr. Lond. 180–189.
Thakur, J.K., Han, J., Parsons, R.L., 2016. Factors influencing deformations of geocell-reinforced recycled asphalt pavement bases under cyclic loading. J. Mater. Civ. Eng. 29 (3), 04016240.
Webster, S.L., Alford, S.J., 1978. Investigation of Construction Concepts for pavements Across Soft Ground. U.S. Army Engineer Waterways Experiment Station, Washington D.C.
Yang, X., 2010. Numerical Analyses of Geocell-reinforced Granular Soils under Static and Repeated Loads. Ph.D. dissertation. The University of Kansas.
Yang, X., Han, J., Parsons, R.L., Leshchinsky, D., 2010. Three-dimensional numerical modeling of single geocell-reinforced sand. Front. Archit. Civ. Eng. China 4 (2), 233–240.
Yuu, J., Han, J., Rosen, A., Parsons, R.L., Leshchinsky, D., 2008. Technical review of geocell-reinforced base courses over weak subgrade. In: First Pan Am.erican Geosynthetics Conference, Cancun, Mexico, pp. 2–5.
Zhou, H., Wen, X., 2008. Model studies on geogrid- or geocell-reinforced sand cushion on soft soil. Geotext. Geomembranes 26 (3), 231–238.